CONFERENCE PRE-PRINT

Non-Inductive Current Start-up and Optimized Ramp-up in EXL-50U for Next-Generation Spherical Torus Devices

Xinchen JIANG [1,2], Yuejiang SHI [2*], Xianming SONG [2], Wenjun LIU [2], Guang YANG [2], Xiang GU [2], Yapeng ZHANG [2], Ji QI [2], Dong GUO [2], Shaodong SONG [2], Zhenxing WANG [2], D Banerjee [3], Y-K Martin PENG [2], Xianmei Zhang [1*]

[1] School of Physics, East China University of Science and Technology, Shanghai 200237, China
[2] Hebei Key Laboratory of Compact Fusion, ENN Science and Technology Development Co., Ltd, Langfang, China
[3] DISAT, Polytechnic University of Turin, Torino 10129, Italy

Email: jiangxinchen2025@gmail.com & yjshi@ipp.ac.cn

Abstract

The paper report the successful realization of a 1 MA hydrogen–boron ($p–^{11}B$) discharge in the ENN Xuanlong-50U(EXL-50U) spherical torus (ST), enabled by electron cyclotron resonance heating (ECRH) non-inductive in a trapped particle configuration (TPC), followed by a current ramp-up optimized through the synergistic use of ECRH and central solenoid (CS) drive. A boron-rich fueling scheme, using 30% diborane and real-time boron powder injection, increased the initial current ramp-up rate by 78% relative to hydrogen-only plasmas. Stable and repeatable operation at the 1 MA level was achieved, supported by active control of the ramp-up rate. Through the synergy of EC and CS and the adjustment of the balanced configuration, the discharge success rate of EXL-50U approached 100%, with the current rapidly ramping from 20 kA to 1 MA. The fastest ramp-up speed reached 7 MA/s, with an average ramp-up rate of 3.4 MA/s. These findings establish an integrated approach to high current operation in ST, combining electron generation across a wide energy spectrum (from eV to MeV), real-time boronization, and a coordinated EC and CS ramp-up strategy, offering a viable pathway for future fusion reactors

Keywords: spherical torus, Hydrogen-Boron plasma, Non-Inductive Current Start-up

1. INTRODUCTION

ENN Xuanlong-50U (EXL-50U) spherical torus (ST) is an upgraded version of the ENN Xuanlong-50 (EXL-50) device. Since its establishment in 2022, it has completed over 30,000 discharges. EXL-50U alone has performed more than 13,000 discharges and has reached a plasma current (Ip) of up to 1 MA by 2025[1].

In the optimization research of tokamak start-up and ramp-up, experiments on EXL-50 have shown that electron cyclotron wave (ECW) can effectively drive current, especially in low-density plasma, where the averaged current drive effectiveness on EXL-50 is around 1 A/W[2]. The current in EXL-50 is mainly carried by energetic electrons (a wide energy spectrum from eV to MeV), which are accelerated under multi-harmonic resonance conditions. In EXL-50, low-frequency whistler waves driven by energetic electrons were observed[3,4]. Using a 50 GHz ECW system, a current of about 120 kA can be achieved at higher densities, significantly improving the current drive efficiency. The computed thermal and energetic electron fluids can have quite different parameters, the latter fluid containing a clear large relativistic effect. [5]. The cause-and-effect analysis of the EXL-50 device shown in Fig. 1 reveals the key mechanisms of non-inductive current drive under central solenoid-free (CS-free) conditions, indicating that the external vertical magnetic field (IPF5/6) exhibits the strongest causal correlation with the plasma current.

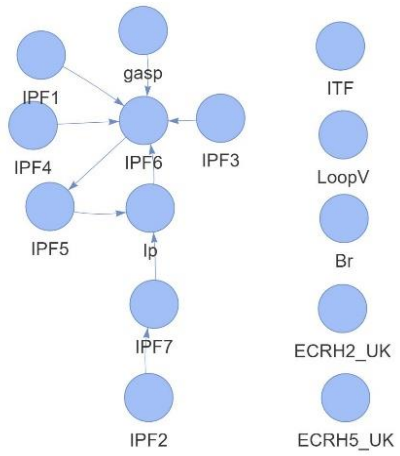

FIG. 1. Cause-and-effect Diagram about EXL-50

The combination of energetic electron generation via multi-harmonic ECRH, real-time boron fueling, and current ramp-up using both central solenoid (CS) and non-inductive methods, along with the synergistic interaction of CS, poloidal field (PF), and EC, provides a validated framework for reactor-relevant applications. This framework addresses two long-standing challenges in ST development:

- The limited volt-second (Vs) budget inherent to compact ST geometry,
- The compatibility of impurity control and heating constraints during the start-up and current ramp-up phases.

As compact ST devices evolve toward fully superconducting systems with constrained flux budgets, and as advanced fuels like p–11B demand greater purity and heating control. To achieve high-performance plasmas and maintain the advantages of hydrogen-boron spherical tokamaks in future devices like ENN He Long-2 (EHL-2), further optimization of plasma start-up, ramp-up, and high confinement operation phases, along with refined discharge and control strategies, is necessary. This is crucial not only for ensuring the success of flat-top phase physics experiments but also for advancing the hydrogen-boron ($p–^{11}B$) fusion path for ST toward higher current parameters (I_p ~ 3 MA)[6]. EXL-50U's operational regime provides both a validated physics basis and an engineering template. The integrated strategies demonstrated here could serve as a foundation for future ST programs, including EHL-2[7] and STEP[8].
This paper is organized as follows. Section 2 provides the early discharge optimized framework. Section 3 outlines the experimental analysis and optimization plan for EXL-50U, clearly presenting our results on EXL-50U. Section 4 introduces the 1 MA discharge achievement. Section 5 concludes with a summary and future plans.

2. EARLY DISCHARGE OPTIMIZED FRAMEWORK

Firstly, it is necessary to clarify the influence of each model on the weighting of the overall framework. To minimize ambiguity in terminology and ensure accuracy of the discussion while maintaining a clear physical picture.
In this paper, the discharge process is divided into the following stages: the non-inductive start-up phase, the early phase prior to magnetic surface evolution, the current ramp-up phase during which the last closed flux surface (LCFS) gradually expands or stabilizes, the flat-top phase, and the ramp-down phase. The flat-top and ramp-down phases are beyond the scope of this discussion.
During the non-inductive start-up phase, the PF is kept as constant as possible. At this time, the electron cyclotron (EC) system is the only source term, carrying out non-inductive current initiation within the pre-formed magnetic field configuration. Therefore, the key optimization factors at this stage are the resonance layer between the toroidal field (B_t) and EC [9], as well as the trapped particle configuration (TPC)[9].
The early phase prior to magnetic surface evolution is characterized by the acceleration of energetic electrons within the vacuum vessel. EC waves, undergoing multiple reflections and absorption by the metal wall of the vacuum vessel at high multi-harmonic resonances, significantly increase the efficiency of energetic electron acceleration, with energies typically ranging from keV to MeV. These energetic electrons contribute to the formation of the LCFS and are well confined under the TPC configuration[10]. Due to the asymmetric effect of their orbits, these electrons carry current at the LCFS boundary. This means that during the calculation process, the edge current profile can be sharpened to more accurately describe the current distribution. Therefore, the main variables during this stage include the total EC power, deposition location, and the absorption that increases as the plasma expands overall. At this stage, EXL-50U do not have sufficient diagnostics to distinguish whether the heating is dominated by ohmic heating or EC heating, nor to clearly determine how the current profile has been modified. However, it can be established that this stage has an upper limit for Ip, which is lower than the current driven by ohmic heating. Therefore, further optimization does not result in a significant order-of-magnitude improvement.
When the LCFS forms and gradually expands to the preset configuration, the PF switches to control, with the primary change source coming from the CS coils and plasma density. At this point, a stable plasma is achieved, and the overall plasma parameters satisfy the conditions for Ohmic heating. At this stage, reliable equilibrium reconstructions can be performed using EFIT, which are consistent with magnetic diagnostics.
Visible-light images captured during the non-inductive start-up phase, the early phase prior to magnetic surface evolution, the current ramp-up phase during which the last closed flux surface (LCFS) gradually expands (Fig. 2) confirm the progressive evolution of the plasma boundary structure. The observed changes in plasma cross-section are consistent with the SE[11]-reconstructed equilibrium.

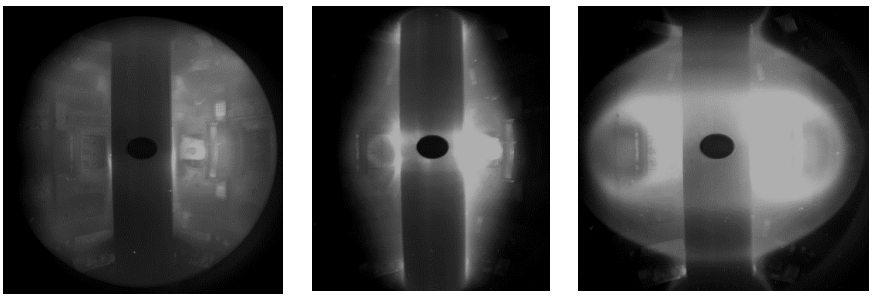

Fig. 2. Visible-light camera sequence showing the evolution of plasma shape during current ramp-up.

3. EXPERIMENTAL ANALYSIS AND OPTIMIZATION OF EXL-50U

EXL-50U is a low-aspect-ratio ST (major radius R = 0.6 m, minor radius a ≈ 0.45 m, $B_t \leq 1.2$ T), equipped with five electron cyclotron gyrotrons that provide up to 1 MW of microwave heating power—two operating at 50 GHz and three at 28 GHz[12]. Based on previous experimental results on EXL-50, reliable non-inductive start-up can be achieved when 3–4 resonance layers are present in the vacuum vessel.

By adjusting the toroidal field to B_t = 1.0 T, 50 GHz EC enables multi-harmonic resonance absorption (Fig. 3). Compared with the 28 GHz scheme at lower B_t, the 50 GHz configuration significantly improves the formation of non-inductive current. Multiple harmonic layers are observed to overlap within the vacuum vessel, which strongly supports efficient electron acceleration.

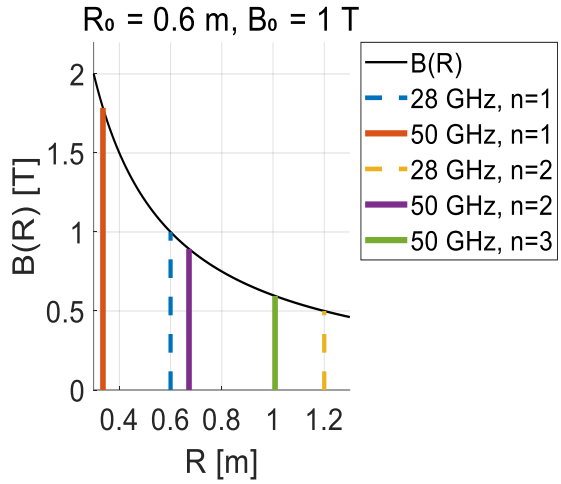

Fig. 3. EC wave resonance area at B0 = 1T

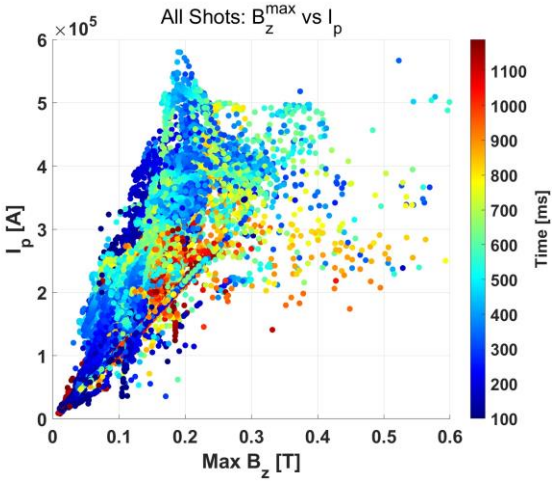

Fig. 4. The plasma current vs max vertical field Bz

As shown in Fig. 4, valid discharges selected shots of EXL-50U were used for statistical analysis, covering plasma currents in the range of 20–580 kA. Scatter plots of plasma current against the maximum vertical field show a clear positive correlation. The scatter distribution demonstrates a clear positive correlation between the maximum vertical field (max B_z) and the plasma current (Ip). In particular, higher vertical fields are consistently associated with the formation of larger plasma currents, while lower B_z values correspond to a wider spread and reduced stability. The color-coded time evolution further reveals that the correlation is most prominent during the early 0–200 ms phase, where enhanced vertical field shaping strongly supports current initiation.

Experimental observations also show that the EC-driven current in EXL-50U deviates from the conventional I_{ECCD} scaling, pointing to distinct physics of energetic electron confinement in ST geometry. However, due to the absence of inductive diagnostics in EXL-50U, a strict quantitative validation cannot yet be performed.

This experimental evidence can be further interpreted within the framework of generalized plasma equilibrium theory. The development of plasma equilibrium from open-field to closed-flux configurations is governed by the balance among plasma current, vertical field, and pressure contributions. The generalized Shafranov force-balance relation can be written as: $2\pi R I_p B_z = (\mu_0/2) G I_p^2 + 4S < p >$.where μ_0 the vacuum permeability, and S<*p*> the pressure-related surface integral. The geometric factor G is defined as: $G = ln(8R/a) + li/2 - 3/2$. Vertical field shaping is thus identified as a critical factor for current evolution: increasing PF coil bias to strengthen the vertical field is positively correlated with improved early current formation, consistent with theoretical predictions. with li being the normalized internal inductance[13]. Therefore, B_z shaping is identified as a key factor in current evolution: increasing PF coil bias to strengthen the vertical field is positively correlated with improved early current formation, consistent with theoretical predictions. This relation provides a theoretical explanation for the strong correlation observed in Fig. 4: a stronger B_z not only facilitates early plasma current initiation but also ensures consistency of global equilibrium in ST geometry.

3.1 Non-inductive start-up phase

In the experimental analysis and optimization of EXL-50U, the TPC has been employed as a key strategy for non-inductive plasma start-up, in contrast to the traditional Field Null Configuration (FNC).The advantages of TPC are threefold. First, the magnetic mirror effect effectively suppresses radial and vertical particle losses, thereby increasing electron density and temperature during the non-inductive phase. Second, TPC broadens the operational parameter space, allowing for stable initiation over a wider range of filling gas pressures and vertical field strengths. Third, due to its higher non-inductive current-drive efficiency, TPC enables shorter start-up times compared with FNC, thereby reducing CS flux consumption and improving volt-second efficiency. These features have also been validated in other devices such as K-STAR[9], where TPC enabled reliable low-voltage start-up and expanded operational flexibility. This distinction has proven crucial for optimizing both plasma current formation and the

subsequent ramp-up rate, although detailed physical models of key factors, such as the parallel electric field ($E_{\parallel}$), remain under active investigation.

As shown in shot #4744 (Fig. 5), pure EC injection of 160 kW at 28 GHz from the equatorial launch initiated a plasma current of about 20 kA at around –250 ms, even before the CS was applied. When CS assistance followed, the plasma current continued to rise. However, during the flat portion of the pure EC phase, the current gradually decreased, indicating that further optimization is required. To address this, future experiments will shorten the transition time between pure EC start-up and ramp-up, thereby improving efficiency and reducing unnecessary energy consumption. The vertical red dashed line in Fig. 5 marks the onset of CS current. The waveforms from top to bottom are: (a) plasma current, (b) gyrotron anode high voltage, (c) flux consumption of CS coils, (d) toroidal electric field, which remains below 0.15 V/m throughout the entire ramp-up phase, and (e) line-integrated density. Notably, the induced loop voltage (E_{loop}) is far below the ohmic breakdown threshold, indicating that conventional Townsend-type ohmic breakdown is not applicable under these conditions.

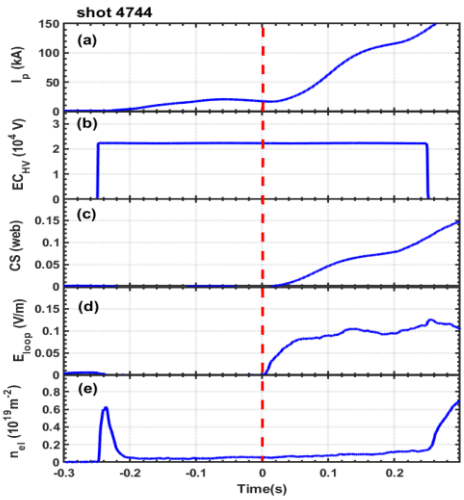

Fig. 5. Typical start-up waveforms with 28 GHz ECRH in EXL-50U [1]. The vertical red dashed line indicates the start of CS current. Waveforms from top to bottom are: (a) plasma current; (b)gyrotron anode high voltage; (c) flux consumption of CS coils; (d) toroidal electric field which is below 0.15V/m in whole ramp-up phase (e) line integrated density.

During the non-inductive phase, both hydrogen (H_2) and diborane (B_2H_6) were tested as fueling gases. Although calculations suggested that B_2H_6 injection would increase radiative losses compared with H_2, no significant difference was observed experimentally, likely because the 50 GHz ECH power already exceeded the breakdown threshold. Consequently, H_2 was chosen as the standard pre-fill gas to maximize the probability of successful breakdown and stable start-up.

3.2 The early phase prior to magnetic surface evolution

To eliminate interference from the CS and isolate non-inductive effects, dedicated experiments were conducted on EXL-50U focusing solely on the synergy between EC and PF coil shaping. In this configuration, the role of EC power and its deposition is particularly critical. The metallic wall of the vacuum vessel enables multiple reflections and enhances absorption at high multi-harmonic resonances, thereby increasing the efficiency of accelerating energetic electrons with energies typically ranging from keV to MeV. These electrons contribute to the formation of LCFS and are well confined under the TPC. Due to the asymmetric nature of their orbits, they drive boundary currents at the LCFS, effectively sharpening the edge current profile. Thus, the main control parameters in this stage are the total EC power, its deposition location, and the evolving absorption characteristics as the plasma expands.

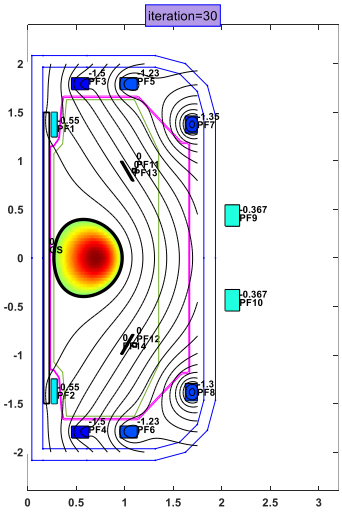

Fig. 6 (a) . #9390 plasma current to 40 kA

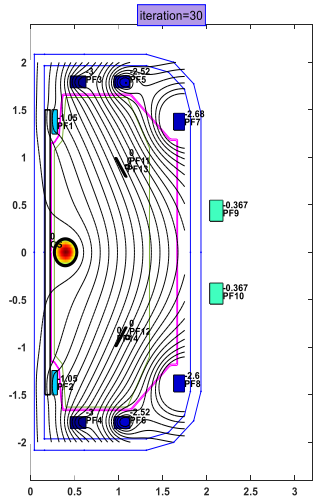

(b) . With #9390 increased PF7–10 negative settings, resulting in an Ip increase to 60 kA.

As shown in Fig. 6, pure 28 GHz ECRH non-inductive start-up generated plasma currents of about 40 kA. When negative PF7–10 coil currents were increased, the vertical field was strengthened and the plasma current rose to ~60 kA even without CS assistance, demonstrating the critical role of vertical field shaping. In practice, optimized PF settings require PF 7–8 to carry approximately twice the current of PF 9–10 to ensure favorable vertical equilibrium for TPC operation. Although current diagnostics are insufficient to unambiguously distinguish between Ohmic and EC-dominated heating, or to fully resolve the current profile modifications, it is clear that the plasma current Ip in this phase is capped below the PF-driven value due to limited EC power and spatial constraints. Therefore, while optimization of EC and PF synergy does not yield order-of-magnitude increases in current, it plays a decisive role in determining the ramp-up speed and volt-second efficiency.

The evolution of the poloidal flux distribution under different PF coil settings is illustrated in Fig. 7. Compared with the weaker vertical field case (left, reduced negative PF 7–10 currents), the stronger vertical field case (right, increased negative PF 7–10 currents) shows compressed contours near the vessel wall and PF coils, indicating a steeper $|\nabla\psi|$ and stronger vertical field B_z . The magnetic axis shifts and tilts relative to the chamber geometry, reflecting changes in longitudinal force balance and vertical equilibrium. In addition, the flux surfaces near the top and bottom edges move closer to the wall and bend more strongly, implying a compressed boundary layer that reduces early plasma–wall interaction. These changes enhance mirror ratio and particle confinement, thereby supporting non-inductive current initiation and ramp-up under TPC conditions.

Complementary diagnostics using hard X-ray (HXR) spectra (Fig. 8) at 200–220 ms revealed distinct signatures of energetic electron confinement under different PF and ECRH conditions. The slope of the HXR spectrum correlates with the presence of energetic electrons, indicating that the achievable plasma current is closely linked to the balance between PF-driven vertical field shaping and ECRH-driven energetic electron generation.

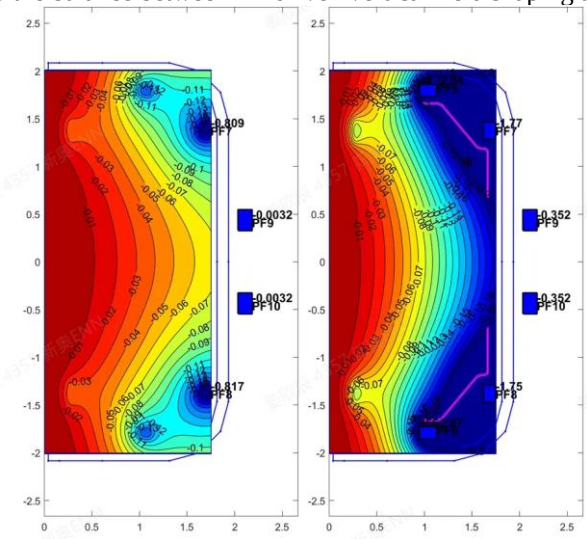

Fig. 7. Poloidal flux (ψ) distributions in EXL-50U under different PF coil conditions. (Left) Reduced negative PF7–10 currents lead to weaker vertical field and broader flux surfaces. (Right) Increased negative PF7–10 currents compress the flux contours and enhance vertical confinement.

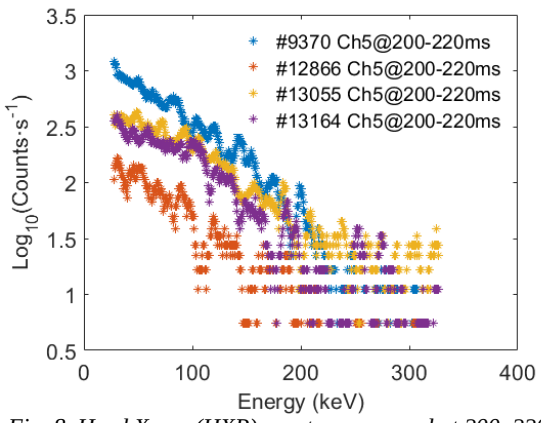

Fig. 8. Hard X-ray (HXR) spectra measured at 200–220 ms under different shots in EXL-50U.

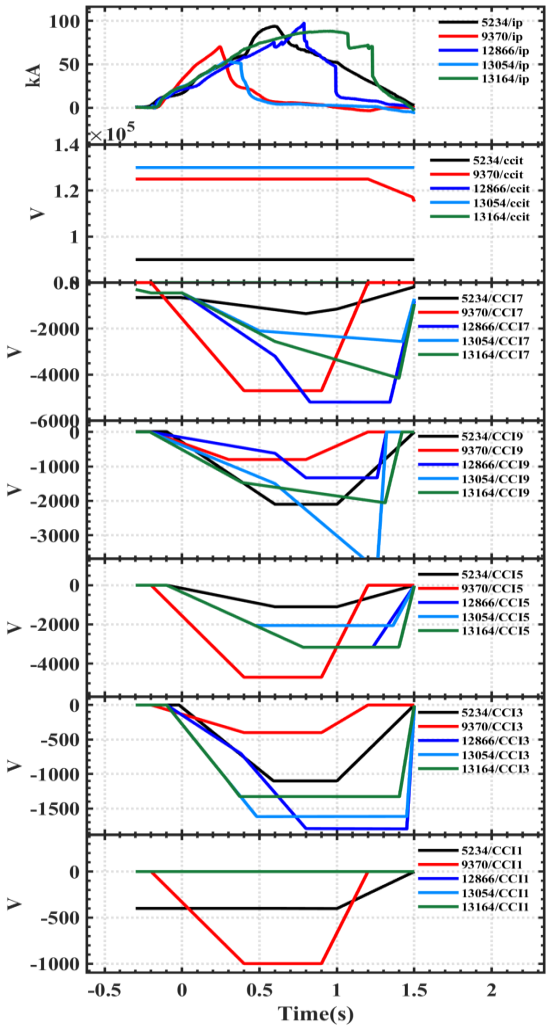

Fig. 9. non-inductive start-up optimization with TPC under different shots in EXL-50U

Fig.9 results highlight that efficient ramp-up in EXL-50U requires coordinated optimization of PF coil current shaping, ECRH power deposition. While ECRH alone is sufficient to generate 100kA of current, the addition of optimized PF fields and staged CS drive enables higher currents, reduced flux consumption, and improved stability. Overall, TPC has played a central role in EXL-50U experiments, enabling efficient, repeatable, and stable non-inductive plasma initiation. By combining optimized PF coil settings, 50 GHz ECH, and precise fueling control, EXL-50U demonstrates the operational advantages of TPC in advancing spherical tokamak non-inductive start-up physics.

3.3 The ramp-up phase

Optimization of the current ramp-up rate is essential, as excessively slow ramp-up prolongs plasma–wall interactions, leading to impurity accumulation and reduced conductivity, while excessively fast ramp-up can trigger skin effects, steep current gradients, magnetohydrodynamic (MHD) instabilities, or runaway electron generation. In EXL-50U, dedicated experiments have demonstrated that a balanced ramp-up can be achieved through the synergistic operation of ECRH, the CS, and optimized PF coil currents.
As shown in Fig. 10, 50 GHz ECRH alone produced a plasma current of ~64 kA, which was subsequently amplified to ~160 kA by applying a staged negative CS pulse. These results clearly confirm that coordinated ECRH and CS strategies significantly enhance ramp-up performance, enabling efficient and stable plasma initiation under reactor-relevant conditions. Furthermore, complementary experiments revealed that the relative timing between ECRH and CS assistance plays a decisive role. As illustrated in Fig. 11, three dedicated shots were performed with delay times ΔT_{CS-EC} of 50, 100, and 250 ms between the onset of ECRH and the application of CS drive. The shortest delay (shot 5090, $\Delta T \approx 50$ ms) yielded the lowest plasma current (~120 kA), whereas longer delays (shots 5100 and 5120) resulted in progressively higher Ip values. These findings demonstrate that extending the transition interval between EC initiation and CS drive enhances ramp-up efficiency, increases plasma current, reduces unnecessary flux consumption, and stabilizes current evolution. The fastest ramp-up rate reached 7 MA/s.

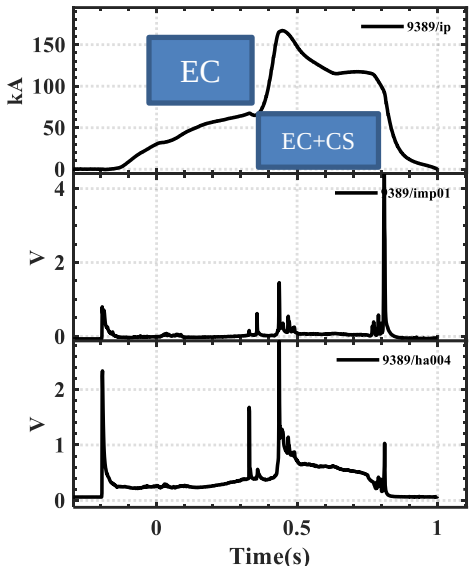

Fig. 10. Plasma current ramp-up by EC alone and by EC+CS synergy. 50 GHz ECRH alone generated ~64 kA of plasma current, which was amplified to ~160 kA by applying a staged negative CS pulse(imp01:O).

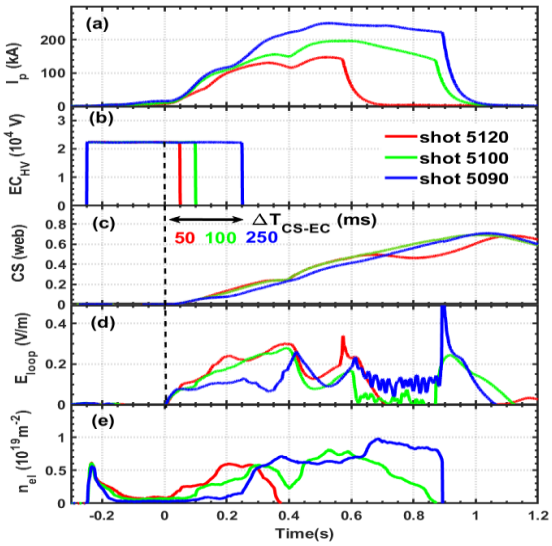

Fig. 11. Dedicated shots for the verification of synergetic effects between ECRH and CS. The vertical black dashed line indicates the start of CS current. Waveforms from top to bottom are: (a) plasma current; (b) gyrotron anode high voltage; (c) flux consumption of CS coils; (d) toroidal electric field; (e) line integrated density.

These results demonstrate that coordinated ECRH and CS strategies can significantly enhance ramp-up performance in spherical tokamaks, enabling efficient and stable plasma initiation under reactor-relevant conditions.

4. 1 MA DISCHARGE ACHIEVEMENT

Using the optimized EC start-up combined with CS-assisted ramp-up, EXL-50U has reproducibly achieved 1 MA hydrogen–boron discharges. A controlled CS swing from +30 kA to –40 kA was applied, consuming approximately 1.08 Vs (~90% of the available flux). Combined with boron-rich fueling (30% B_2H_6 + 70% H_2) and synchronized boron injection, enhanced the initial ramp-up rate by 78%, reaching 3.4 MA/s within the first 70 ms. During this stage, Thomson scattering measurements indicated a core electron temperature exceeding 3 keV with

a line-averaged density of ~1 × 10^{19} m^{-3}. Under lower-density conditions, the core temperature further peaked at 3.5 keV, demonstrating strong energetic electron heating and efficient power coupling in the early ramp-up phase. More importantly, Continuous 50 GHz ECRH operation, Fig. 12 compares the radial profiles of electron density, electron temperature, EC power deposition, and driven current for X-mode [Fig. 12(a)] and O-mode [Fig. 12(b)] injection in EXL-50U. In both cases, the density and temperature profiles exhibit peaked cores (~1.4 × 10^{19} m^{-3} and 3 keV, respectively) that decrease toward the edge. However, clear differences emerge in the EC absorption and current drive characteristics.

For the X-mode case, the absorbed power is relatively weak (~15% total absorption), producing a modest deposition peak near ρ ≈ 0.5. The resulting bipolar current distribution arises from the competition between the Fisch–Boozer and Ohkawa mechanisms, indicating limited net coupling efficiency and partial cancellation in the driven current profile.

By contrast, the O-mode case shows a much higher absorption fraction (~57%), with deposition strongly localized around ρ ≈ 0.5 and a nearly unipolar current profile. This concentrated deposition greatly enhances non-inductive current drive capability.

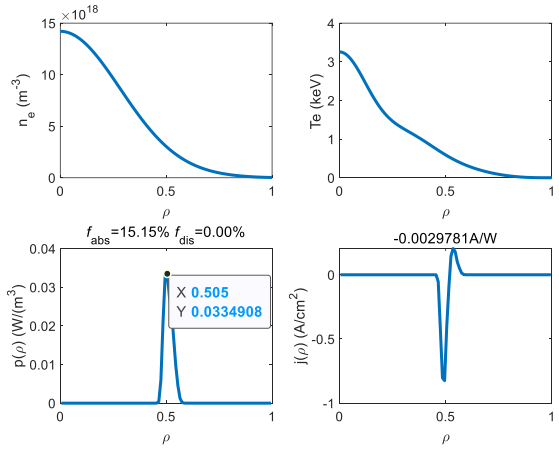

Fig. 12(a). X-mode simulation: central electron density and temperature profiles, with power deposition broadly distributed around ρ ≈ 0.5 (peak ~0.03 W/m³) and a bipolar driven-current distribution. The total absorption fraction is about 15%.

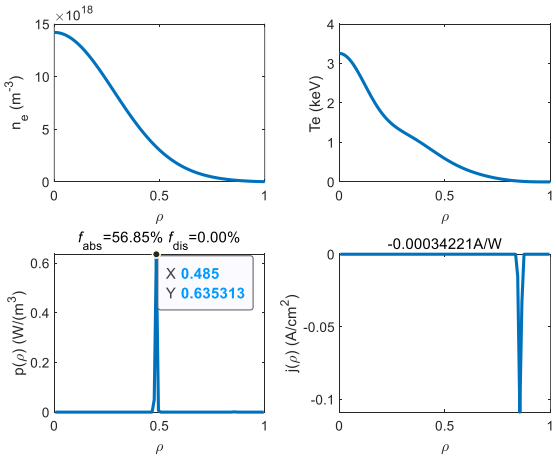

Fig. 12(b). O-mode simulation: more concentrated power deposition at ρ ≈ 0.5 (peak ~0.64 W/m³) with a nearly unipolar driven-current profile. The total absorption fraction reaches 57%, indicating much stronger coupling efficiency.

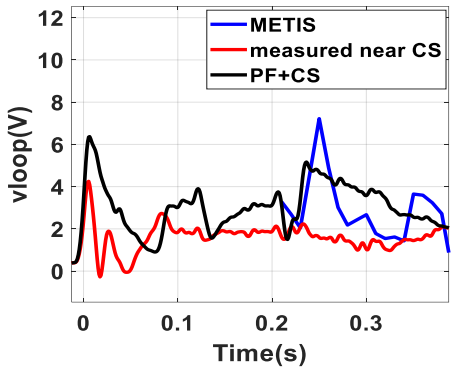

Fig. 12(c). Loop voltage decomposition: comparison between measured loop voltage near CS, reconstructed PF+CS contribution, and METIS simulation, highlighting the dominant role of non-inductive processes during early current formation.

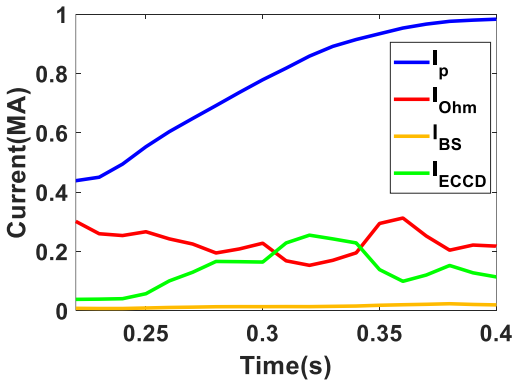

Fig. 12(d). Time evolution of plasma current components in a 1 MA EXL-50U discharge, showing contributions from total plasma current (Ip), Ohmic current (Iohm), bootstrap current (IBS), and ECCD.

Despite partial CS assistance, loop voltage decomposition (Fig. 12(c)) shows that non-inductive processes contributed early current formation. The decomposition satisfies the relation $V_{PF+CS} - V_{meas} = V_{eddy} + V_{plasma} + \Delta V_{geom/diag}$ where V_{eddy} denotes the induced voltage from eddy currents in the conducting wall, V_{plasma} represents contributions from plasma-driven non-inductive processes, and $\Delta V_{geom/diag}$ accounts for geometric and diagnostic uncertainties.

During t = 0.05–0.21 s, the PF+CS expected voltage was approximately twice the measured value, providing clear evidence of strong EC-driven non-inductive current drive at this stage.

For $t > 0.21$ s, METIS simulations indicate that the contribution from traditional ECCD ray-tracing calculations (genray) was only about 10% As shown in Fig. 12(d), the Ohmic current contribution remained around 30%, while the EC-driven component exhibited substantial fluctuations. These results confirm the hybrid non-inductive/inductive ramp-up nature of the discharge. Although conventional theory predicts poor EC drive efficiency and weak absorption, experimental conditions revealed significant enhancement due to mode conversion, Doppler effects, and multi-scale interactions. Multi-fluid equilibrium calculations further suggest that energetic electrons carried up to 90% of the total plasma current, with the remainder mainly attributed to energetic electrons (further validation is ongoing).

5. SUMMARY AND FUTURE PLANS

The non-inductive start-up in EXL-50U was driven by 230 kW of top-launched 50 GHz ECRH in a TPC, which directly performed non-inductive plasma initiation without any applied loop voltage. This equilibrium, combined with boron-rich fueling (30% B_2H_6 + 70% H_2) and synchronized boron injection, enhanced the initial ramp-up rate by 78%, reaching 3.4 MA/s within the first 70 ms. With CS assistance, EXL-50U reproducibly achieved 1 MA hydrogen–boron discharges, marking a significant milestone in spherical tokamak research.
Dedicated experiments further demonstrated that:

- TPC outperforms FNC by broadening operational windows, reducing PF flux consumption, and ensuring stable non-inductive initiation.
- PF coil shaping is critical in the early phase: optimized vertical fields compress flux surfaces, enhance mirror ratio, and improve confinement, supporting faster and more stable ramp-up.
- ECRH–CS synergy enables efficient current amplification: the relative timing between EC initiation and CS drive was found to decisively control ramp-up efficiency, flux usage, and current stability.
- Loop voltage decomposition and METIS simulations confirmed that non-inductive processes dominated early current formation

The EXL-50U results establish a volt-second–efficient and reproducible pathway spanning the non-inductive start-up phase, the early stage preceding magnetic surface formation, and the ramp-up phase. This integrated approach provides a transferable framework for advanced spherical tokamak concepts. In particular, the findings are directly relevant to STEP, EHL-2, and compact p–11B reactor designs, where robust non-inductive start-up, reliable energetic electron confinement, and boron-rich fueling will be essential to achieving reactor-relevant performance.

REFERENCES

[1] SHI Y, 2025 Achievement of 1 MA discharges in hydrogen–boron plasmas in the EXL-50U *Plasma Sci. Technol.* **27** 092002
[2] Shi Y, 2022 Solenoid-free current drive via ECRH in EXL-50 spherical torus plasmas *Nucl. Fusion* **62** 086047
[3] Guo D, 2022 Experimental study of the characteristics of energetic electrons outside LCFS in EXL-50 spherical torus *Plasma Phys. Control. Fusion* **64** 055009
[4] Wang M, 2023 Generation of energetic electrons by an electron cyclotron wave through stochastic heating in a spherical tokamak *J. Plasma Phys.* **89** 905890603
[5] Banerjee D, 2022 Investigation of the effectiveness of 'multi-harmonic' electron cyclotron current drive in the non inductive EXL-50 ST *J. Phys.: Conf. Ser.* **2397** 012011
[6] Jiang X 2025 Physics design of current drive and strategy of heating system for EHL-2 spherical torus *Plasma Sci. Technol.* **27** 024012
[7] Liu M, 2024 ENN's roadmap for proton-boron fusion based on spherical torus *Physics of Plasmas* **31** 062507
[8] Nilima A, 2025 Optimisation of STEP poloidal field coils with superconducting coil constraints in STEP-Bluemira power plant design framework *Fusion Engineering and Design* **220** 115357
[9] An Y, 2017 Efficient ECH-assisted plasma start-up using trapped particle configuration in the versatile experiment spherical torus *Nucl. Fusion* **57** 016001
[10] Ishiguro M, 2012 Non-inductive current start-up assisted by energetic electrons in Q-shu University experiment with steady-state spherical tokamak *Phys. Plasmas* **19**
[11] Anon 2019 First plasma scenario development for HL-2M *Fusion Engineering and Design* **147** 111254
[12] SHI Y *Overview of EXL-50U Experiments: Addressing Key Physics Issues for Future Spherical Torus Reactors* (IAEA)
[13] Maekawa T, Uchida M and Tanaka H 2018 Non-inductive build-up of a hot plasma by X-wave ECH/ECCD to remove initial high loop-voltage from start-up of fusion tokamaks *Nucl. Fusion* **58** 016037